

High p_T correlated tests of lepton universality in lepton(s) + jet(s) processes; an EFT analysis

Yoav Afik,^{1,*} Shaouly Bar-Shalom,^{1,†} Jonathan Cohen,^{1,‡} Amarjit Soni,^{2,§} and Jose Wudka^{3,¶}

¹*Physics Department, Technion–Institute of Technology, Haifa 3200003, Israel*

²*Physics Department, Brookhaven National Laboratory, Upton, NY 11973, US*

³*Physics Department, University of California, Riverside, CA 92521, USA*

(Dated: November 9, 2020)

We suggest a new class of tests for searching for lepton flavor non-universality (LFNU) using ratio observables and based on correlations among the underlying LFNU new physics (NP) effects in several (seemingly independent) di-lepton and single lepton + jet(s) processes. This is demonstrated by studying the effects generated by LFNU 4-Fermi interactions involving 3rd generation quarks. We find that the sensitivity to the scale (Λ) of the LFNU 4-Fermi operators significantly improves when the correlations among the various di-lepton + jets and single-lepton + jets processes are used, reaching $\Lambda \sim \mathcal{O}(10)$ TeV at the HL-LHC.

Intriguing hints of lepton-flavor non-universality (LFNU) and therefore of new physics (NP) have appeared in recent years in neutral and charged semileptonic B-decays [1–21] (for a recent review see [22]): the $R_{K^{(*)}}$ and $R_{D^{(*)}}$ anomalies which occur in $b \rightarrow s\ell^+\ell^-$ and $b \rightarrow c\ell^-\nu_\ell$ transitions, respectively.

In this work, we consider testing for LFNU in lepton(s) + jets production at the LHC, by exploiting correlations amongst several LFNU observables. Specifically, we show that an enhanced sensitivity to the scale of the NP can be obtained by combining multiple LFNU tests, based on ratio observables. We demonstrate this for two specific new physics (NP) scenarios, using the so-called SM Effective Field Theory (SMEFT) framework [23–26], although this approach can be extended to establish a more systematic mapping between the underlying NP dynamics and experimentally realistic observables. The importance of using correlations in the search for NP has recently gained some attention, e.g., in leptoquark searches by combining di-lepton and single lepton production channels [27] and in top-quark systems by using measurements from different top production and decay processes to probe the NP effects [28–31].

Any evidence of possible LFNU phenomena contradicts the key Standard Model (SM) prediction that the differences in the rates of processes differing only in the flavor of the leptons involved are suppressed by small differences in the Yukawa couplings. In this sense lepton flavor is an accidental (approximate) symmetry of the SM, which may be strongly violated in a variety of well-motivated NP scenarios. Hence, even if the current experimental indications of LFNU have not yet met discovery criteria, providing an accurate probe of these processes, whether confirming such indications or not, will provide a better understanding of the flavor structure of the physics beyond the SM.

Let us denote generic lepton(s) + jets processes as follows:

$$\begin{aligned} (mnp)_{\ell\ell} : pp &\rightarrow \ell_i^+ \ell_i^- + m \cdot j + n \cdot j_b + p \cdot t \\ (mnp)_\ell : pp &\rightarrow \ell_i^\pm + m \cdot j + n \cdot j_b + p \cdot t + \cancel{E}_T, \end{aligned} \quad (1)$$

where m is the number of light jets (j), n is the number of b-jets (j_b) and p is the number of top or anti-top quarks in the final state of the leading-order (LO) hard process; \cancel{E}_T denotes missing transverse energy, associated with final state neutrinos. We then define two classes of generic LFU tests at the LHC, involving ratios of the charged di-lepton and single-lepton production channels in (1), normalized to the corresponding electron-production channels:

$$T_{\ell\ell}^{mnp} = \frac{\sigma_{\ell\ell}^{mnp}}{\sigma_{ee}^{mnp}}, \quad T_\ell^{mnp} = \frac{\sigma_\ell^{mnp}}{\sigma_e^{mnp}}, \quad (2)$$

where $\sigma_{\ell\ell}^{mnp}$ and σ_ℓ^{mnp} are the total cross-sections of the processes $(mnp)_{\ell\ell}$ and $(mnp)_\ell$ in (1), respectively. Lepton flavor violation effects of the type $pp \rightarrow \ell_i \ell_j + \dots$ ($i \neq j$) will not be considered here. For LFNU processes with only neutrinos in the final state, ratios such as (2) are not useful, since the neutrino flavor cannot be detected. In this case a different strategy is needed, which we briefly discuss below. Note that ratio observables such as in (2) provide more reliable probes of NP, since they potentially minimize the effects of theoretical uncertainties involved in the calculation of the corresponding cross-sections. For example, the NLO QCD and, e.g. loop corrections from EFT

* yoavafik@campus.technion.ac.il

† shaouly@physics.technion.ac.il

‡ jcohen@campus.technion.ac.il

§ adlersoni@gmail.com

¶ jose.wudka@ucr.edu

operators (see [32]), are expected to be cancelled to a large extent in our ratio observables, as will all lepton-flavor independent corrections. Even so, the impact of the theoretical uncertainties is accounted for in our analysis, as a part of the total systematic uncertainties that we consider below. Indeed, different variations of ratio observables have been used in recent years for LFNU studies in top-quark decays [33] and B physics [17–19, 34–41].

In the SM (or within NP scenarios which conserve lepton flavor universality) we have $T_{\ell\ell}^{mnp}, T_\ell^{mnp} \rightarrow 1$, since, as noted above, deviations from unity can only be generated through the non-universal Higgs-lepton Yukawa couplings and through lepton mass dependent polynomials and logarithms from higher order corrections. The former is proportional to the lepton masses and is therefore negligible, while the latter are much smaller than the expected experimental accuracy – as is the case, *in particular*, for high p_T events which is of our interest in this work. We will include non-universal reconstruction efficiencies for the different leptonic final states in the overall uncertainty of the measurement of $T_{\ell\ell, \ell}^{mnp}$ defined in (2).

As mentioned earlier, we describe the underlying NP responsible for $T_{\ell\ell}^{mnp} \neq 1$ and $T_\ell^{mnp} \neq 1$, using the SMEFT framework, defined by adding to the SM Lagrangian an infinite series of higher-dimensional, gauge-invariant operators, $\mathcal{O}_i^{(n)}$. These operators are constructed using the SM fields and their coefficients are suppressed by inverse powers of the NP scale M [23–26]:

$$\mathcal{L} = \mathcal{L}_{SM} + \sum_{n=5}^{\infty} \frac{1}{M^{n-4}} \sum_i f_i \mathcal{O}_i^{(n)}, \quad (3)$$

where n is the mass dimension of $\mathcal{O}_i^{(n)}$ and we assume decoupling and weakly-coupled heavy NP, so that n equals the canonical dimension. The dominating NP effects are then expected to be generated by contributing operators with the lowest dimension (smallest n) that can be generated at tree-level in the underlying theory. The (Wilson) coefficients f_i depend on the details of the underlying heavy theory and, therefore, parameterize all possible weakly-interacting and decoupling types of heavy physics.

In what follows we will consider the leading dimension six operators ($n = 6$) and drop the index n .¹ We also define the “effective scale” $\Lambda = M/\sqrt{|f|}$ whence

$$f/M^2 = \eta_f/\Lambda^2, \quad (4)$$

where $\eta_f = \pm 1$ denotes the sign of f . Thus, for example, $\Lambda = M$ for “natural” NP with $|f| = 1$, which we will assume throughout the rest of this work, unless stated otherwise.

TABLE I: The potentially lepton non-universal dimension six operators in the SMEFT (using the Warsaw basis [26], see also text). The subscripts p, r, s, t are flavor indices.

Higgs-Lepton scalar	Higgs-Lepton vector	Lepton MDM
$\mathcal{O}_{eH}(pr) \left (H^\dagger H)(\bar{l}_p e_r H) \right.$	$\mathcal{O}_{Hl}^{(1)}(pr) \left (H^\dagger i \overleftrightarrow{D}_\mu H)(\bar{l}_p \gamma^\mu l_r) \right.$	$\mathcal{O}_{eW}(pr) \left (\bar{l}_p \sigma^{\mu\nu} e_r) \tau^I H W_{\mu\nu}^I \right.$
	$\mathcal{O}_{Hl}^{(3)}(pr) \left (H^\dagger i \overleftrightarrow{D}_\mu^I H)(\bar{l}_p \tau^I \gamma^\mu l_r) \right.$	$\mathcal{O}_{eB}(pr) \left (\bar{l}_p \sigma^{\mu\nu} e_r) H B_{\mu\nu} \right.$
	$\mathcal{O}_{He}(pr) \left (H^\dagger i \overleftrightarrow{D}_\mu H)(\bar{e}_p \gamma^\mu e_r) \right.$	
4 – Fermi : $(\bar{L}L)(\bar{L}L)$	4 – Fermi : $(\bar{R}R)(\bar{R}R)$	4 – Fermi : $(\bar{L}L)(\bar{R}R)$
$\mathcal{O}_{lq}^{(1)}(prst) \left (\bar{l}_p \gamma_\mu l_r)(\bar{q}_s \gamma^\mu q_t) \right.$	$\mathcal{O}_{eu}(prst) \left (\bar{e}_p \gamma_\mu e_r)(\bar{u}_s \gamma^\mu u_t) \right.$	$\mathcal{O}_{lu}(prst) \left (\bar{l}_p \gamma_\mu l_r)(\bar{u}_s \gamma^\mu u_t) \right.$
$\mathcal{O}_{lq}^{(3)}(prst) \left (\bar{l}_p \gamma_\mu \tau^I l_r)(\bar{q}_s \gamma^\mu \tau^I q_t) \right.$	$\mathcal{O}_{ed}(prst) \left (\bar{e}_p \gamma_\mu e_r)(\bar{d}_s \gamma^\mu d_t) \right.$	$\mathcal{O}_{ld}(prst) \left (\bar{l}_p \gamma_\mu l_r)(\bar{d}_s \gamma^\mu d_t) \right.$
		$\mathcal{O}_{qe}(prst) \left (\bar{q}_p \gamma_\mu q_r)(\bar{e}_s \gamma^\mu e_t) \right.$
4 – Fermi : $(\bar{L}R)(\bar{R}L) + \text{h.c.}$	4 – Fermi : $(\bar{L}R)(\bar{L}R) + \text{h.c.}$	
$\mathcal{O}_{ledq}(prst) \left (\bar{l}_p^j e_r)(\bar{d}_s q_{tj}) \right.$	$\mathcal{O}_{lequ}^{(1)}(prst) \left (\bar{l}_p^j e_r) \epsilon_{jk} (\bar{q}_s^k u_t) \right.$	
	$\mathcal{O}_{lequ}^{(3)}(prst) \left (\bar{l}_p^j \sigma_{\mu\nu} e_r) \epsilon_{jk} (\bar{q}_s^k \sigma^{\mu\nu} u_t) \right.$	

¹ There is a single lepton number violating dimension five operator in the SMEFT framework, the so called Weinberg operator $\bar{\ell}^c \tilde{H}^* \tilde{H}^\dagger \ell$ [42], for which the scale Λ is very large and is therefore not relevant for this study.

In Table I we list all the dimension six operators that can potentially violate LFU and that are, therefore, relevant for this study; operators with four leptons are excluded and we also assume that baryon number is conserved in the underlying heavy theory. Here, we will demonstrate our strategy for the two specific SU(2) triplet and singlet 4-Fermi operators ($prst$ are flavor indices):

$$\mathcal{O}_{lq}^{(3)}(prst) = (\bar{l}_p \gamma_\mu \tau^I l_r) (\bar{q}_s \gamma^\mu \tau^I q_t) , \quad (5)$$

$$\mathcal{O}_{qe}(prst) = (\bar{e}_q \gamma_\mu e_r) (\bar{q}_s \gamma^\mu q_t) , \quad (6)$$

focusing on the case where the heavy underlying NP has a LFNU coupling to 3rd generation quarks and 2nd generation leptons, i.e., on $\mathcal{O}_{lq}^{(3)}(2233)$ and $\mathcal{O}_{qe}(2233)$; it should be understood, though, that similar effects can be generated in the electron and τ -lepton channels, though, the phenomenology and detection strategies of final states involving the τ -leptons are fundamentally different from those involving the electrons and muons. Note also that we will adopt a "one-coupling-scheme", i.e, we will study the effects of one operator at the time. The reasoning behind focusing on one type of NP is that, in general, the scales and dynamics of the NP that underlies the different operators may vary, so that "injecting" into the processes considered below more than one type of NP requires additional assumptions regarding the energy scales and the signs and sizes of the corresponding Wilson Coefficients.

We will not consider operators that have a flavor changing quark current involving the 3rd generation quarks, e.g., $\mathcal{O}_{lq}^{(3)}(2232)$ and $\mathcal{O}_{lq}^{(3)}(3332)$, which can generate the $b \rightarrow s\mu^+\mu^-$ and $b \rightarrow c\tau^-\bar{\nu}_\tau$ transitions and may, therefore, contribute to $R_{K^{(*)}}$ and $R_{D^{(*)}}$, respectively. These operators can generate LFNU collider signals similar to those studied here, see e.g., [43–45]. For example, $\mathcal{O}_{lq}^{(3)}(2232)$ generates the $\mu^+\mu^-\bar{s}b$ and $\mu^+\mu^-\bar{c}t$ contact terms with the same effective scale, which can contribute to the ratio observables $T_{\mu\mu}^{010}$ and $T_{\mu\mu}^{001}$, via $sg \rightarrow b\mu^+\mu^-$ and $cg \rightarrow t\mu^+\mu^-$, respectively. Furthermore, the operator $\mathcal{O}_{lq}^{(3)}(3332)$ generates the contact interactions $\tau^+\tau^-\bar{s}b$, $\tau^-\bar{\nu}_\tau\bar{s}t$ and $\tau^+\nu_\tau\bar{c}b$, which can contribute to the T -tests $T_{\tau\tau}^{010}$, $T_{\tau\tau}^{110}$ as well as T_τ^{010} , T_τ^{110} via the hard processes $sg \rightarrow b\tau^+\tau^-$, $gg \rightarrow \bar{s}b\tau^+\tau^-$ and $cg \rightarrow \bar{b}\tau^-\bar{\nu}_\tau$, $gg \rightarrow \bar{c}b\tau^-\bar{\nu}_\tau$, respectively.

To study the sensitivity to the flavor non-universal NP we define the following χ^2 -test:²

$$\chi^2 = \sum_X \frac{[T_{\ell\ell}^X(\Lambda) - T_{\ell\ell}^{X,\text{exp}}]^2}{(\delta T^X)^2} + \sum_Y \frac{[T_\ell^Y(\Lambda) - T_\ell^{Y,\text{exp}}]^2}{(\delta T^Y)^2} , \quad (7)$$

where $X, Y \in (m, n, p)$ denote the $\ell\ell$ and single ℓ channels, respectively, and $\delta T^X, \delta T^Y$ denote the corresponding total experimental plus theoretical 1σ uncertainties, which are assumed to be statistically independent (the experimental uncertainties are assumed to be the dominant ones, see also discussion above).

For the purpose of exacting a bound on Λ we assume that, on average, no NP is observed. We thus generate $\mathcal{O}(10000)$ random realizations of the sets of "measured" T -tests, $T_{\ell\ell}^{X,\text{exp}}$ and $T_\ell^{Y,\text{exp}}$ [to be used for the χ^2 -test in (7)], normally distributed with average 1 (i.e., the SM prediction) and standard deviation δT :³

$$T_{\ell\ell}^{X,\text{exp}} = \mathcal{N}\left(1, (\delta T^X)^2\right), \quad T_\ell^{Y,\text{exp}} = \mathcal{N}\left(1, (\delta T^Y)^2\right) . \quad (8)$$

where $\mathcal{N}(a, s^2)$ denotes the normal distribution for average a and standard deviation s .

The overall uncertainties δT^X and δT^Y of the data samples are taken as:

$$\delta T^{X,Y} = \sqrt{(\delta T_{\text{stat}}^{X,Y})^2 + (\delta T_{\text{sys}}^{X,Y})^2} , \quad (9)$$

where $\delta T_{\text{stat}}^{X,Y}$ and $\delta T_{\text{sys}}^{X,Y}$ stand for the statistical and systematic uncertainties expected in the data samples, respectively. The statistical uncertainties are estimated from the expected number of events based on the SM cross-sections: $\delta T_{\text{stat}}^X = \sqrt{2/N_{\ell\ell}^X(SM)}$ and $\delta T_{\text{stat}}^Y = \sqrt{2/N_\ell^Y(SM)}$; for the systematic uncertainties we analyse below 3 different cases: $\delta T_{\text{sys}}^{X,Y} = 5\%, 10\%, 15\%$ for channels involving only light-jets and/or b-jets in the final state and $\delta T_{\text{sys}}^{X,Y} = 10\%, 20\%, 30\%$ for channels with a top-quark in the final state. Without knowing the actual uncertainties

² In the general case, where the correlation matrix for the systematic uncertainties is provided, the χ^2 -test reads instead (e.g., for the di-muon channels): $\chi^2 = \sum_{ij} (T_{\ell\ell}^{X_i}(\Lambda) - T_{\ell\ell}^{X_i,\text{exp}}) \sigma_{X_i X_j}^{-2} (T_{\ell\ell}^{X_j}(\Lambda) - T_{\ell\ell}^{X_j,\text{exp}})$, where $\sigma_{X_i X_j}^{-2} = (\delta T^{X_i} \rho^{X_i X_j} \delta T^{X_j})^{-1}$ and $\rho^{X_i X_j}$ is the correlation matrix provided by the experiment (see also discussion below).

³ Due to the different detection efficiencies of electrons and muons, we expect the ratios $T_{\ell\ell,\ell}^{\text{exp}}$ to deviate from unity even in the absence of NP. This, however, has no effect on our χ^2 -test analysis and will not change our main results.

of the experiment, the uncertainty scenarios outlined above serve as realistic benchmarks for conveying the main message of this work. In particular, we assume that they account for both the experimental and the theoretical uncertainties, while the latter are expected to be minimized due to the use of ratio observables (see also discussion above). Moreover, we assume (in Eq. (7)) that the systematic uncertainties are uncorrelated, since the information about the correlation matrix of the uncertainties is not yet available for the measurements/channels used in our χ^2 -test (see also footnote 2). We note, though, that correlations among the systematic uncertainties in the various channels used below will degrade the sensitivity to the NP, since they effectively reduce the number of observables/channels. For example, a 100% correlation among the uncertainties of the di-muon channels used below is equivalent to using a single channel, and that can cause a dramatic loss of sensitivity as is shown in Fig.1, i.e., comparing the sensitivity to Λ with $m_{\ell\ell}^{\min} = 700$ GeV with that of Λ with $m_{\ell\ell}^{\min} = 800$ GeV.

The expected bounds on Λ are then extracted from the randomly distributed range of best fitted values of Λ that minimize the χ^2 -test of Eq. (7) (an example is shown in Appendix A). We use three LHC integrated luminosity scenarios: $\mathcal{L} = 140, 300, 3000$ [fb] $^{-1}$, corresponding to the currently accumulated LHC plan, the RUN3 projections and the planned HL-LHC luminosity, respectively. Then, based on the SM cross-sections, we demand at least 100 events for any of the channels $X, Y \in (m, n, p)$, i.e., $\sigma^{SM} \cdot \mathcal{L} > 100$, or else this channel is not included in the χ^2 -test of Eq. (7). This 100 event criterion is set to ensure that the potential reducible backgrounds (see discussion below) will be sub-leading and, therefore, have a small impact on the overall uncertainty in these measurements.

We demonstrate below our formalism for detecting LFNU based on the ratio observables of (2), using the QCD generated (and therefore dominant) exclusive di-muon + multi-jet and/or top-quarks channels:⁴

$$\begin{aligned}
(010)_{\mu\mu} &: pp \rightarrow \mu^+ \mu^- + j_b \\
(110)_{\mu\mu} &: pp \rightarrow \mu^+ \mu^- + j + j_b \\
(020)_{\mu\mu} &: pp \rightarrow \mu^+ \mu^- + 2 \cdot j_b \\
(002)_{\mu\mu} &: pp \rightarrow \mu^+ \mu^- + t\bar{t},
\end{aligned} \tag{10}$$

where the LFNU effects are generated by the operators $\mathcal{O}_{lq}^{(3)}(2233)$ and $\mathcal{O}_{qe}(2233)$ (i.e., the cross-sections involving electrons in the denominator of $T_{\mu\mu}^{mnp}$ in (2) are assumed to be SM-like). We can then define a generic form for the cross-section in (10) with a cut $m_{\ell\ell} > m_{\ell\ell}^{\min}$ on the di-muon invariant mass:

$$\sigma_{\ell\ell}^{mnp}(m_{\ell\ell}^{\min}) = \sigma_{\ell\ell}^{\text{SM},mnp}(m_{\ell\ell}^{\min}) + \frac{\sigma_{\ell\ell}^{\text{INT},mnp}(m_{\ell\ell}^{\min})}{\Lambda^2} + \frac{\sigma_{\ell\ell}^{\text{NP},mnp}(m_{\ell\ell}^{\min})}{\Lambda^4}, \tag{11}$$

where σ^{INT} and σ^{NP} are the SM \times NP interference and NP² terms, respectively. The dominant NP contribution then depends on the di-lepton invariant mass cut and the di-lepton channel involved. In particular, the $\mathcal{O}(\Lambda^{-2})$ correction, σ^{INT} , dominates for moderate di-lepton invariant mass cut, for which the SM term is appreciable, whereas the $\mathcal{O}(\Lambda^{-4})$ NP² correction, σ^{NP} , is dominant in the high $m_{\ell\ell}^{\min}$ -cut regime, where the SM contribution is suppressed. We thus obtain a better sensitivity to the NP with higher $m_{\ell\ell}^{\min}$ -cuts (see below), for which the signal-to-background ratio is significantly improved.

All cross-sections contributing to the LFU T -tests in (2) were calculated exclusively (i.e., separately for each channel without matching) using MADGRAPH5_AMC@NLO [48] at LO parton-level and a dedicated universal FeynRules output (UFO) model for the EFT framework was produced using FEYNRULES [49], where we have assumed for simplicity that the NP effects reside in the muonic operators, so that the cross-sections involving electrons are SM-like. In addition, the LO MSTW 2008 parton distribution functions (PDF) set (MSTW2008lo68cl [50])⁵ in the 5 flavor scheme was used with a dynamical scale choice for the central value of the factorization (μ_F) and renormalization (μ_R) scales, corresponding to the sum of the transverse mass in the hard-process. As a baseline selection, we used the default MADGRAPH5_AMC@NLO parameters: $p_T > 20$ GeV and $|\eta| < 5$ for jets, $p_T > 10$ GeV and $|\eta| < 2.5$ for leptons. The minimum angular distance in the $\eta - \phi$ plane between all objects (leptons and jets) is > 0.4 . Finally, kinematic selections cuts (e.g., on the di-lepton invariant mass) were imposed using MADANALYSIS5 [51].

Before presenting our results, we would like to address the validity of our EFT analysis, in particular, in connection to the high $m_{\ell\ell}^{\min}$ regime and the role of the higher-dimensional operators in the EFT expansion of (11). This has two aspects (see also [52]): (i) the validity of the EFT expansion in $1/\Lambda$, i.e., in terms of the scale of the higher dimension operators, and (ii) the validity of the specific cross-section calculations within the EFT prescription. In particular, as mentioned above, the SM \times NP interference term is significantly suppressed with the high $m_{\ell\ell}^{\min}$ cut that we use

⁴ We do not consider here Drell-Yan di-lepton production $pp \rightarrow \ell^+ \ell^-$, i.e., with no jet activity, which correspond to the LFNU signal test $T_{\ell\ell}^{000}$ and which, in our case, are generated by b-quark fusion and are, therefore, sub-leading. Such Drell-Yan processes were studied within the SMEFT framework and in connection to LFNU physics and the B-anomalies in [35, 46, 47], where bounds on the corresponding 4-Fermi operators were derived (see also discussion below).

⁵ We note that our results, which are based on ratio observables, are insensitive to the PDF choice (within the uncertainties considered), in particular, since the PDF choice is lepton universal and, therefore, has a similar effect on final states with different lepton generations.

and, so, the leading effect comes from the NP² which is $\propto \Lambda^{-4}$. The next term in the EFT expansion would be the SM \times NP(dim.8) contribution, where NP(dim.8) stands for dimension eight operators, so that this contribution is also $\propto \Lambda^{-4}$. However, since the SM \times NP(dim.8) terms are proportional to the SM amplitude, they are subject to the same suppression at high $m_{\ell\ell}^{\min}$ cuts and their contribution is, therefore, expected to be even smaller than the sub-leading SM \times NP(dim.6) in (11). In this sense our EFT expansion is valid, even though the NP² term dominates.

As for the validity of the calculation within the EFT framework: this is a more subtle issue, since it depends on the details of the underlying theory. Namely, the validity of the EFT calculation naively requires the overall energy flow in the underlying scattering process to be smaller than the NP threshold, i.e., that $\sqrt{\hat{s}} < \Lambda$, to ensure that the heavy excitations from the underlying NP cannot be produced on-shell. In our case, we find that the sensitivity to the NP (i.e., the bounds) reaches $\Lambda \sim 3 - 6$ TeV for underlying NP couplings of $\mathcal{O}(1)$, i.e., for a Wilson coefficient $f = 1$. Thus, the EFT prescription is valid since the bulk of the generated events are clustered below $\sqrt{\hat{s}} \sim 3 - 4$ TeV, due to the energy limitations of the 14 TeV LHC. Also, if the underlying NP couplings correspond to e.g., $f = 2$, then our bounds apply to a NP scale of $M = \sqrt{2} \cdot \Lambda$ (see (4)), so that the EFT validity in this case is further expanded to higher c.m. energies. Furthermore, in some instances the EFT approach may hold even if the overall energy flow is larger than the NP scale; for example, if the heavy NP is being exchanged in the t-channel, so that the energy flow through the heavy propagator is effectively lower than $\sqrt{\hat{s}}$, in which case the EFT prescription also holds when $\sqrt{\hat{s}} > \Lambda$. Thus, as mentioned above, the consistency of the calculation within the EFT framework as well as the legitimacy of the NP bounds depend on how one interprets the details of the underlying theory [52] (see also [32]).

Using the four di-lepton + jets channels in (10), we show in Fig. 1 and Table II a sample of the resulting expected 95% confidence level (CL) bounds on scales of the operators $\mathcal{O}_{lq}^{(3)}$ (2233) and \mathcal{O}_{qe} (2233), as a function of the di-muon invariant mass cut $m_{\ell\ell}^{\min}$. In particular, the Monte Carlo χ^2 -test analysis of LFNU was repeated for different values of $m_{\ell\ell}^{\min}$, for the three integrated luminosity cases $\mathcal{L} = 140, 300, 3000$ [fb]⁻¹ and the three systematic uncertainty cases, which yield an overall uncertainty of $\delta T \sim 10\%, 15\%, 20\%$ for the di-muon multi-jets production channels (010) _{$\mu\mu$} , (110) _{$\mu\mu$} and (020) _{$\mu\mu$} , i.e., with no top quarks in the final state. The (002) _{$\mu\mu$} di-muon + top-pair production channel in (10) was not included in the χ^2 -test analysis used to derive the 95% CL bounds listed in Table II, as it does not pass the 100 event criterion for the $(\mathcal{L}/[fb^{-1}], m_{\mu\mu}^{\min}/[GeV]) = (140, 300), (300, 400), (3000, 700)$ cases considered in this Table. This process, i.e., $pp \rightarrow \ell^+\ell^- + t\bar{t}$, is, however, an important channel that might prove to be a promising direction for the future for disentangling various other types of NP effects, e.g., in leptoquark searches [53, 54]. Note also the sharp drop at $m_{\mu\mu}^{\min} = 800$ GeV, which is caused as a result of our 100 events criteria. In particular, at $m_{\mu\mu}^{\min} = 800$ GeV only the (020) _{$\mu\mu$} channel produces more than 100 events (hence the much lower sensitivity to the NP scale), whereas for $m_{\mu\mu}^{\min} \leq 700$ GeV all three channels with no top-quarks in the final state, i.e., (010) _{$\mu\mu$} , (110) _{$\mu\mu$} and (020) _{$\mu\mu$} , pass the 100 events criteria.

We see that, as expected, the sensitivity to the underlying NP depends on the sign of the Wilson coefficients $\eta_f = \pm 1$ and on the overall uncertainty, and it varies with the di-muon invariant mass cut. We find, for example, that with the current LHC accumulated luminosity of $\mathcal{L} = 140$ [fb]⁻¹, the best 95% CL bounds are obtained with the cut $m_{\mu\mu}^{\min} = 300$ GeV: $\Lambda \gtrsim 2.3 - 3.4$ TeV for $\mathcal{O}_{lq}^{(3)}$ (2233) and $\Lambda \gtrsim 2.4 - 4.2$ TeV for \mathcal{O}_{qe} (2233), depending on the overall systematic uncertainty and on the sign of η_f . Also, a much higher sensitivity is expected at the HL-LHC with a tighter cut of $m_{\ell\ell}^{\min} = 700$ GeV, reaching up to $\Lambda \gtrsim 6.5$ TeV for $\mathcal{O}_{lq}^{(3)}$ (2233) with $\eta_f = +1$ and \mathcal{O}_{qe} (2233) with $\eta_f = -1$.

TABLE II: The expected 95% CL bound on the scale (in TeV) of the operators $\mathcal{O}_{lq}^{(3)}$ (2233) and \mathcal{O}_{qe} (2233) (in parenthesis), for di-muon invariant mass cuts $m_{\mu\mu} > 300, 400$ and 700 GeV which are applied for an integrated luminosity of $\mathcal{L} = 140, 300$ and 3000 [fb]⁻¹, respectively. Results are shown for $\eta_f = \pm 1$ and three values of the overall uncertainty of $\delta T \sim 10\%, 15\%$ and 20%, corresponding to the three systematic uncertainty cases 1,2, and 3. For all cases considered in the table only the channels (010) _{$\mu\mu$} , (110) _{$\mu\mu$} and (020) _{$\mu\mu$} pass the 100 criteria. See also text.

	95% CL bounds: $\Lambda_{\mathcal{O}_{lq}^{(3)}(2233)} (\Lambda_{\mathcal{O}_{qe}(2233)})$ [TeV]					
	$\mathcal{L} = 140$ [fb] ⁻¹		$\mathcal{L} = 300$ [fb] ⁻¹		$\mathcal{L} = 3000$ [fb] ⁻¹	
	$m_{\mu\mu}^{\min} = 300$ GeV		$m_{\mu\mu}^{\min} = 400$ GeV		$m_{\mu\mu}^{\min} = 700$ GeV	
	$\eta_f = +1$	$\eta_f = -1$	$\eta_f = +1$	$\eta_f = -1$	$\eta_f = +1$	$\eta_f = -1$
$\delta T \sim 10\%$ (case 1)	3.4(2.6)	3.2(4.2)	4.1(3.1)	3.9(4.9)	6.3(4.4)	6.0(6.4)
$\delta T \sim 15\%$ (case 2)	3.0(2.5)	2.7(3.8)	3.7(3.0)	3.3(4.5)	5.8(4.2)	5.5(5.9)
$\delta T \sim 20\%$ (case 3)	2.6(2.4)	2.3(3.4)	3.3(2.9)	2.9(4.2)	5.1(4.1)	4.7(5.5)

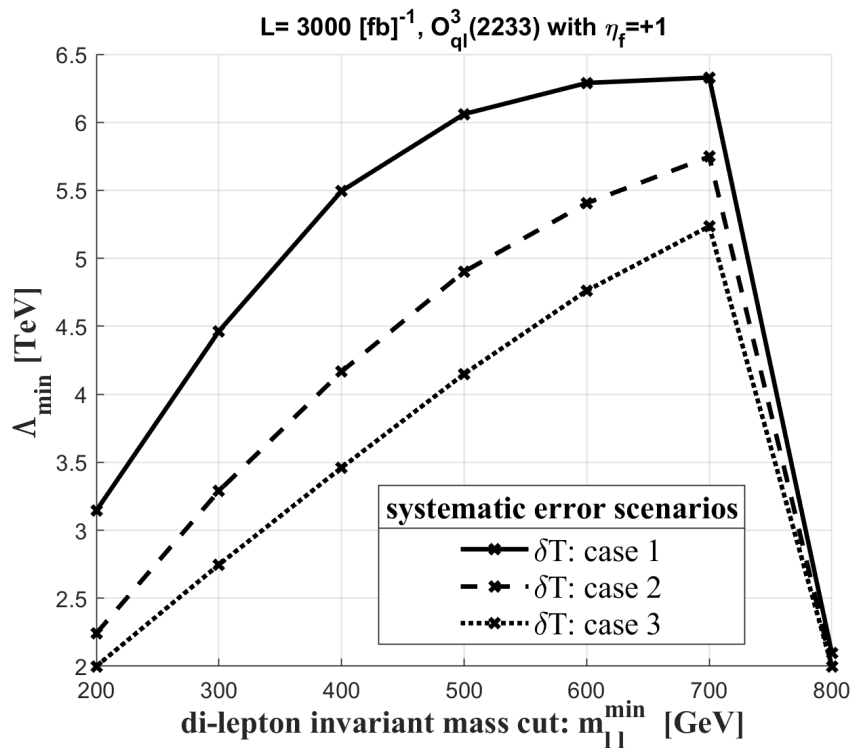


FIG. 1: Expected 95% CL bounds on the scale of the SU(2)-triplet operator $\mathcal{O}_{lq}^{(3)}(2233)$ with $\eta_f = +1$, as a function of the di-lepton invariant mass cut $m_{\ell\ell}^{\min}$, for the HL-LHC with an integrated luminosity of $3000 [\text{fb}]^{-1}$. Results are shown for three overall uncertainty scenarios: δT cases 1-3. See also text.

We now consider a complementary analysis where, instead of examining the bounds under the assumption of no NP in the data, we ask what is the discovery potential of a given NP scenario if the NP is assumed to be present in the data. We thus assume that the experimentally measured ratios $T_{\ell\ell}^{X,\text{exp}}$ are controlled by the NP, so that, in this case, they are normally distributed with a mean value corresponding to the NP expectations $T(\bar{\Lambda})$:

$$T_{\ell\ell}^{X,\text{exp}} = \mathcal{N}\left(T_{\ell\ell}^X(\bar{\Lambda}), (\delta T^X)^2\right), \quad (12)$$

where here $\bar{\Lambda}$ is the value of the NP scale injected into the data and tested against the SM prediction. As for the overall uncertainties, δT^X , we follow the prescription of (9), where this time the statistical uncertainties are assumed to reflect the NP data, i.e., $\delta T_{\text{stat}}^X = \sqrt{2/N^X(\bar{\Lambda})}$, where $N^X(\bar{\Lambda})$ are the number of events expected for a NP scale $\bar{\Lambda}$ in each of the di-lepton channels $X \in (mnp)$. The systematic uncertainties, δT_{sys}^X , are kept unchanged, i.e., using the three cases $\delta T_{\text{sys}}^X = 5\%, 10\%, 15\%$ for channels involving only light-jets and/or b-jets in the final state. We thus vary Λ in the χ^2 -test of (7) [i.e., with T^{exp} normally distributed around $T(\bar{\Lambda})$ following (12)], from which we generate the distribution of the best fitted NP scale, $\hat{\Lambda}$, for each value of $\bar{\Lambda}$ (an example is shown in Appendix A).⁶ This is repeated for different values of $\bar{\Lambda}$ until we find the value that yields a distribution which deviates from the SM prediction at a given CL ; we denote this value by $\bar{\Lambda}(CL)$. In Table III we list a sample of our results for the discovery potential of the operators $\mathcal{O}_{lq}^{(3)}(2233)$ and $\mathcal{O}_{qe}(2233)$ at the LHC. In particular, we find that a 5σ discovery of the heavy underlying NP that generates these operators can be obtained at the LHC with $\mathcal{L} = 300 \text{ fb}^{-1}$, if its scale is in the range $\bar{\Lambda}(5\sigma) \sim 2.3 - 2.9 \text{ TeV}$ for $\mathcal{O}_{lq}^{(3)}(2233)$ and $\bar{\Lambda}(5\sigma) \sim 2.8 - 3.4 \text{ TeV}$ for $\mathcal{O}_{qe}(2233)$, depending on the uncertainty in the measurement of the ratios $T_{\ell\ell}^{mnp}$. At the HL-LHC, the corresponding discovery potential is extended up to $\bar{\Lambda}(5\sigma) \sim 3.7 - 4.6 \text{ TeV}$.

Let us briefly address the potential background for the multi-jets $\ell^+\ell^-$ production channels $(010)_{\mu\mu}$, $(110)_{\mu\mu}$ and $(020)_{\mu\mu}$ used in our χ^2 -tests. We note that the irreducible background to these processes such as $Z + jets$ and $W + jets$

⁶ In an ideal measurement with $\delta T \rightarrow 0$ we will clearly have $\hat{\Lambda} = \bar{\Lambda}$, so that the NP signal corresponding to any Λ will be well separated from the SM prediction.

TABLE III: The values of the NP scale $\bar{\Lambda}(CL)$ (in TeV) that will yield a 5σ discovery of the the operators $\mathcal{O}_{lq}^{(3)}$ with $\eta_f = +1$ and \mathcal{O}_{qe} with $\eta_f = -1$, at the LHC with $\mathcal{L} = 300 \text{ fb}^{-1}$ and $m_{\mu\mu}^{\min} = 400 \text{ GeV}$ and at the HL-LHC with 3000 fb^{-1} and $m_{\mu\mu}^{\min} = 700 \text{ GeV}$. Numbers are given for the three different overall uncertainties corresponding to cases 1,2,3 of the systematic uncertainties and the channels that pass the 100 criteria for all cases are $(010)_{\mu\mu}$, $(110)_{\mu\mu}$ and $(020)_{\mu\mu}$. See also text.

	5 σ discovery: $\bar{\Lambda}(5\sigma)$ [TeV]			
	$\mathcal{O}_{lq}^{(3)}(\eta_f = +1)$		$\mathcal{O}_{qe}(\eta_f = -1)$	
	300 fb $^{-1}$	3000 fb $^{-1}$	300 fb $^{-1}$	3000 fb $^{-1}$
δT case 1	2.9	4.6	3.4	4.6
δT case 2	2.4	4.1	3.1	4.3
δT case 3	2.3	3.7	2.8	4.1

production, are included in our calculation since they interfere with our signals. As for the reducible background, the dominant ones are single top + W-boson (tW : $pp \rightarrow tW$) and vector-boson pair production (VV : $pp \rightarrow VV$) for the $(010)_{\mu\mu}$ and $(110)_{\mu\mu}$ channels (i.e., for the channels $pp \rightarrow \mu^+\mu^- + j$ and $pp \rightarrow \mu^+\mu^- + j + j_b$). For the $(020)_{\mu\mu}$ channel, $pp \rightarrow \mu^+\mu^- + 2 \cdot j_b$, the tW and VV background are sub-leading and the dominant background comes from the more challenging top-quark pair production ($t\bar{t}$: $pp \rightarrow t\bar{t}$). Note, however, that as opposed to our leading di-lepton signals $(010)_{\mu\mu}$, $(110)_{\mu\mu}$ and $(020)_{\mu\mu}$, the reducible background processes, tW , VV and $t\bar{t}$, involve large missing energy, which is carried by the neutrinos in the final state. Thus, they can be significantly suppressed with a proper selection cut on the missing transverse energy \cancel{E}_T (see also next paragraph) and other acceptance criteria such as lepton isolation criteria (that can be applied to minimize to the few percent level the contamination from fake non-prompt leptons from either a misidentified hadron or a decay product of a heavy or light flavor hadron, see e.g., [55]) as well as properties of the transverse momenta and energy distribution of the final state particles which can be used, e.g., for a better separation of the $t\bar{t}$ background from the di-lepton + jets NP signal, see e.g., [52, 56–58].

To give a flavor of the signal (S) to background (B) handle for our LFNU processes, we have applied the di-lepton invariant mass cuts that we used above for our signals $S = (010)_{\mu\mu}$, $(110)_{\mu\mu}$ and $(020)_{\mu\mu}$ (i.e., $m_{\ell\ell}^{\min} = 300, 400, 700 \text{ GeV}$ for $\mathcal{L} = 140, 300, 3000 \text{ fb}^{-1}$, respectively) and an additional simple pre-selection cut of $\cancel{E}_T < 50 \text{ GeV}$ to the leading background processes mentioned above $B = tW$, VV and $t\bar{t}$ (the missing energy pre-selection have a negligible effect on our signals). We then obtain $B_{(010)_{\mu\mu}} \approx 33, 7.5, 0.5 \text{ [fb]}$, $B_{(110)_{\mu\mu}} \approx 10.3, 3.5, 0.2 \text{ [fb]}$ and $B_{(020)_{\mu\mu}} \approx 319, 106, 7.8 \text{ [fb]}$ for the reducible background to the signal channels $(010)_{\mu\mu}$, $(110)_{\mu\mu}$ and $(020)_{\mu\mu}$, respectively, where the three values are for $m_{\ell\ell}^{\min} = 300, 400, 700 \text{ GeV}$ with $\mathcal{L} = 140, 300, 3000 \text{ fb}^{-1}$, respectively. Thus, using $N_{SD} = S/\sqrt{B + (\sigma_B \cdot B)^2}$ as a signal-to-background sensitivity "measure", where $\sigma_B \cdot B$ stands for the expected systematic uncertainty, and setting $\sigma_B = 10\%$, we obtain for all three integrated luminosity cases considered above $N_{SD} \gtrsim \mathcal{O}(1)$ for the signal channels $(010)_{\mu\mu}$, $(110)_{\mu\mu}$, whereas $N_{SD} \gtrsim \mathcal{O}(0.1)$ for the more challenging $(020)_{\mu\mu}$ channel. Note that the $t\bar{t}$ background also applies to the $(110)_{\mu\mu}$ channel due to non-ideal b-tagging efficiencies, and although it can be dramatically reduced with the dilepton invariant mass cuts and the missing energy pre-selection $\cancel{E}_T < 50 \text{ GeV}$, it is still more challenging and, as mentioned above, it requires a more elaborated study which is beyond the scope of this paper; see for example the study of [52], which considered the effects of the $\ell^+\ell^-\bar{b}b$ contact terms on the $(020)_{\mu\mu}$ channel and performed a detailed signal to background optimization, specifically including the $t\bar{t}$ background.

Finally, we note that an important difference between the two operators $\mathcal{O}_{lq}^{(3)}$ and \mathcal{O}_{qe} with respect to our χ^2 -test, is that the former also gives rise to the single-muon + jets and top-quarks production channels $(mnp)_\mu$ [cf. (1)] and to neutrino pair-production (with \cancel{E}_T signature) in association with jets and top-quarks: $(mnp)_{E_T} : pp \rightarrow m \cdot j + n \cdot j_b + p \cdot t + \cancel{E}_T$. In particular, these $(mnp)_\mu$ and $(mnp)_{E_T}$ processes are correlated with the di-lepton + jets production channels $(mnp)_{\mu\mu}$ discussed above. For this case also the best sensitivity to $\mathcal{O}_{lq}^{(3)}(2233)$ is expected from the processes generated by QCD interactions, which are depicted in Fig. 2. In particular, note that the QCD-generated single-muon production channels involve a single top-quark in the final state: $(001)_\mu$, $(101)_\mu$ and $(011)_\mu$, which affect the ratios T_μ^{001} , T_μ^{101} and T_μ^{011} in (2). Indeed, we find that including these single-muon + top-quark channels in the χ^2 -test of (7) yields a better sensitivity to the scale of this operator, e.g., for the HL-LHC case, yielding bounds which are $\sim 1 \text{ TeV}$ stronger than the ones given in Table II. We Note that searches for these single-lepton signatures are on-going (see e.g., [59]), since they may be important for searches of various different types of NP, e.g., of pair-production of a scalar partner of the top-quark in supersymmetric theories [60].

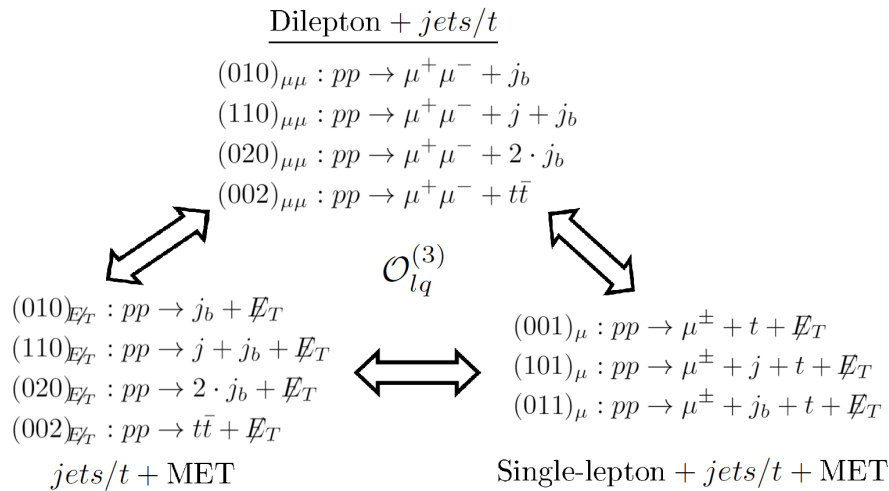


FIG. 2: Correlations among various di-lepton + jets/tops, single-lepton + jets/tops + \cancel{E}_T and jets/tops + \cancel{E}_T (with no charged lepton) processes, which are generated by the SU(2)-triplet-exchange operator

$$\mathcal{O}_{\mu q_3}^{(3)} = (\bar{\mu} \gamma_\mu \tau^I \mu)(\bar{q}_3 \gamma^\mu \tau^I q_3) \text{ via QCD interactions. See also text.}$$

Furthermore, the dominant (QCD generated) neutrino channels are the processes (010) $_{E_T}$, (110) $_{E_T}$, (020) $_{E_T}$ and (002) $_{E_T}$ (see Fig. 2), which can be used as well to obtain a better sensitivity to this operator. This requires, however, a different approach (rather than our χ^2 -tests based on ratio observables) for disentangling the NP effects and will, therefore, not be further investigated here. Note, though, that some of these \cancel{E}_T + jets and/or top-quarks signals are important signals of other well motivated NP scenarios. For example, the processes (020) $_{E_T}$ and (002) $_{E_T}$, i.e., pair production of top-quarks and/or b-jets in association with large \cancel{E}_T , are also signatures of leptoquark pair-production (see e.g., [54, 61]), of pair-production of the scalar partners of the top or bottom quarks in supersymmetric theories (see e.g., [62]) and may also be useful for dark matter searches (see e.g., [63, 64]).

The approach described above improves on the results obtained in previous interesting studies which are based on the analysis of a single process. For example [35] obtains limits of $\Lambda > 1.5 - 1.8$ TeV ($\Lambda > 2.5 - 3$ TeV) at the current LHC (HL-LHC) for the scale of the operators $\mathcal{O}_{lq}^{(3)}(2233)$ and $\mathcal{O}_{qe}(2233)$ in (5) and (6), using Drell-Yan di-lepton production $q\bar{q} \rightarrow \ell^+ \ell^-$; they find a slight improvement for 4-Fermi operators of type $\mathcal{O}(1133)$. Note that the current best bound for this last type of operators, i.e., $\mathcal{O}(1133)$, was obtained at LEP [65–68]: $\Lambda > 0.7 - 2.7$ TeV. We also note that bounds on $\mathcal{O}_{lq}^{(3)}$ derived from the top-quark decays are significantly weaker [69, 70] than ours.

To summarize, we have shown that the lepton flavor non-universal ratio observables $T_{\ell\ell}^{mnp}$ and T_ℓ^{mnp} of (2) can be used to search for new physics using a χ^2 test that is sensitive to the correlations among several lepton + jets and top-quark production channels. We found, for example, that with a realistic assessment of the expected uncertainties involved, a 95%CL bound of $\Lambda \gtrsim 3 - 4$ TeV can be obtained with the current LHC luminosity, while $\Lambda \gtrsim 6 - 7$ TeV is expected at the HL-LHC, for the 4-Fermi operators $\mathcal{O}_{lq}^{(3)}(2233)$ and $\mathcal{O}_{qe}(2233)$ in (5) and (6), which involve 2nd generation leptons and 3rd generation quarks. These bounds are obtained with a generic di-lepton invariant mass cut for all channels, i.e., without any channel-dependent (specific) optimizations that, we believe, can be further used to better isolate the NP effects and, therefore, to obtain an enhanced sensitivity to its scale. Though the above discussion involves only 3rd generation quarks, our multi-channel correlation LFU tests are expected to yield an improved sensitivity also for lepton flavor non-universality new physics which involves the 1st and 2nd quark generations.

ACKNOWLEDGMENTS

We thank Yoram Rozen for useful discussions. The work of AS was supported in part by the U.S. DOE contract #DE-SC0012704.

-
- [1] R. Aaij et al. Differential branching fractions and isospin asymmetries of $B \rightarrow K^{(*)}\mu^+\mu^-$ decays. *JHEP*, 06:133, 2014, 1403.8044.
- [2] Roel Aaij et al. Test of lepton universality using $B^+ \rightarrow K^+\ell^+\ell^-$ decays. *Phys. Rev. Lett.*, 113:151601, 2014, 1406.6482.
- [3] R. Aaij et al. Test of lepton universality with $B^0 \rightarrow K^{*0}\ell^+\ell^-$ decays. *JHEP*, 08:055, 2017, 1705.05802.
- [4] Roel Aaij et al. Angular analysis and differential branching fraction of the decay $B_s^0 \rightarrow \phi\mu^+\mu^-$. *JHEP*, 09:179, 2015, 1506.08777.
- [5] Roel Aaij et al. Angular analysis of the $B^0 \rightarrow K^{*0}\mu^+\mu^-$ decay using 3 fb^{-1} of integrated luminosity. *JHEP*, 02:104, 2016, 1512.04442.
- [6] S. Wehle et al. Lepton-Flavor-Dependent Angular Analysis of $B \rightarrow K^*\ell^+\ell^-$. *Phys. Rev. Lett.*, 118(11):111801, 2017, 1612.05014.
- [7] A. Abdesselam et al. Angular analysis of $B^0 \rightarrow K^*(892)^0\ell^+\ell^-$. In *Proceedings, LHCSki 2016 - A First Discussion of 13 TeV Results: Obergurgl, Austria, April 10-15, 2016*, 2016, 1604.04042.
- [8] The ATLAS collaboration. Angular analysis of $B_d^0 \rightarrow K^*\mu^+\mu^-$ decays in pp collisions at $\sqrt{s} = 8 \text{ TeV}$ with the ATLAS detector. 2017.
- [9] CMS Collaboration. Measurement of the P_1 and P'_5 angular parameters of the decay $B^0 \rightarrow K^{*0}\mu^+\mu^-$ in proton-proton collisions at $\sqrt{s} = 8 \text{ TeV}$. 2017.
- [10] Simone Bifani. Status of New Physics searches with $b \rightarrow s\ell^+\ell^-$ transitions @ LHCb. In *Proceedings, 52nd Rencontres de Moriond on Electroweak Interactions and Unified Theories: La Thuile, Italy, March 18-25, 2017*, pages 197–202, 2017, 1705.02693.
- [11] Roel Aaij et al. Search for lepton-universality violation in $B^+ \rightarrow K^+\ell^+\ell^-$ decays. *Phys. Rev. Lett.*, 122(19):191801, 2019, 1903.09252.
- [12] A. Abdesselam et al. Test of lepton flavor universality in $B \rightarrow K^*\ell^+\ell^-$ decays at Belle. 2019, 1904.02440.
- [13] J. P. Lees et al. Evidence for an excess of $\bar{B} \rightarrow D^{(*)}\tau^-\bar{\nu}_\tau$ decays. *Phys. Rev. Lett.*, 109:101802, 2012, 1205.5442.
- [14] J. P. Lees et al. Measurement of an Excess of $\bar{B} \rightarrow D^{(*)}\tau^-\bar{\nu}_\tau$ Decays and Implications for Charged Higgs Bosons. *Phys. Rev.*, D88(7):072012, 2013, 1303.0571.
- [15] M. Huschle et al. Measurement of the branching ratio of $\bar{B} \rightarrow D^{(*)}\tau^-\bar{\nu}_\tau$ relative to $\bar{B} \rightarrow D^{(*)}\ell^-\bar{\nu}_\ell$ decays with hadronic tagging at Belle. *Phys. Rev.*, D92(7):072014, 2015, 1507.03233.
- [16] S. Hirose et al. Measurement of the τ lepton polarization and $R(D^*)$ in the decay $\bar{B} \rightarrow D^*\tau^-\bar{\nu}_\tau$. *Phys. Rev. Lett.*, 118(21):211801, 2017, 1612.00529.
- [17] Roel Aaij et al. Measurement of the ratio of branching fractions $\mathcal{B}(\bar{B}^0 \rightarrow D^{*+}\tau^-\bar{\nu}_\tau)/\mathcal{B}(\bar{B}^0 \rightarrow D^{*+}\mu^-\bar{\nu}_\mu)$. *Phys. Rev. Lett.*, 115(11):111803, 2015, 1506.08614. [Erratum: *Phys. Rev. Lett.* 115, no. 15, 159901 (2015)].
- [18] R. Aaij et al. Measurement of the ratio of the $B^0 \rightarrow D^{*+}\tau^+\nu_\tau$ and $B^0 \rightarrow D^{*+}\mu^+\nu_\mu$ branching fractions using three-prong τ -lepton decays. *Phys. Rev. Lett.*, 120(17):171802, 2018, 1708.08856.
- [19] R. Aaij et al. Test of Lepton Flavor Universality by the measurement of the $B^0 \rightarrow D^{*+}\tau^+\nu_\tau$ branching fraction using three-prong τ decays. *Phys. Rev.*, D97(7):072013, 2018, 1711.02505.
- [20] Karol Adamczyk. Semitauonic B decays at Belle/Belle II. In *10th International Workshop on the CKM Unitarity Triangle (CKM 2018) Heidelberg, Germany, September 17-21, 2018*, 2019, 1901.06380.
- [21] A. Abdesselam et al. Measurement of $\mathcal{R}(D)$ and $\mathcal{R}(D^*)$ with a semileptonic tagging method. 2019, 1904.08794.
- [22] Simone Bifani, Sébastien Descotes-Genon, Antonio Romero Vidal, and Marie-Hélène Schune. Review of Lepton Universality tests in B decays. *J. Phys. G*, 46(2):023001, 2019, 1809.06229.
- [23] W. Buchmuller and D. Wyler. Effective Lagrangian Analysis of New Interactions and Flavor Conservation. *Nucl. Phys.*, B268:621–653, 1986.
- [24] C. Arzt, M. B. Einhorn, and J. Wudka. Patterns of deviation from the standard model. *Nucl. Phys.*, B433:41–66, 1995, hep-ph/9405214.
- [25] Martin B. Einhorn and Jose Wudka. The Bases of Effective Field Theories. *Nucl. Phys.*, B876:556–574, 2013, 1307.0478.
- [26] B. Grzadkowski, M. Iskrzynski, M. Misiak, and J. Rosiek. Dimension-Six Terms in the Standard Model Lagrangian. *JHEP*, 10:085, 2010, 1008.4884.
- [27] Saurabh Bansal, Rodolfo M. Capdevilla, Antonio Delgado, Christopher Kolda, Adam Martin, and Nirmal Raj. Hunting leptoquarks in monolepton searches. *Phys. Rev. D*, 98(1):015037, 2018, 1806.02370.
- [28] Nathan P. Hartland, Fabio Maltoni, Emanuele R. Nocera, Juan Rojo, Emma Slade, Eleni Vryonidou, and Cen Zhang. A Monte Carlo global analysis of the Standard Model Effective Field Theory: the top quark sector. *JHEP*, 04:100, 2019, 1901.05965.
- [29] Gauthier Durieux, Adrian Irls, Víctor Miralles, Ana Peñuelas, Roman Pöschl, Martín Perelló, and Marcel Vos. The electro-weak couplings of the top and bottom quarks – global fit and future prospects. *JHEP*, 12:098, 2019, 1907.10619.

- [30] Ilaria Brivio, Sebastian Bruggisser, Fabio Maltoni, Rhea Moutafis, Tilman Plehn, Eleni Vryonidou, Susanne Westhoff, and C. Zhang. O new physics, where art thou? A global search in the top sector. *JHEP*, 02:131, 2020, 1910.03606.
- [31] Stefan Birkmann, Johannes Erdmann, Cornelius Grunwald, Gudrun Hiller, and Kevin Kröninger. Correlating uncertainties in global analyses within SMEFT matters. 12 2019, 1912.06090.
- [32] S. Dawson, P.P. Giardino, and A. Ismail. Standard model EFT and the Drell-Yan process at high energy. *Phys. Rev. D*, 99(3):035044, 2019, 1811.12260.
- [33] Jernej F. Kamenik, Andrey Katz, and Daniel Stolarski. On Lepton Flavor Universality in Top Quark Decays. *JHEP*, 01:032, 2019, 1808.00964.
- [34] Elena Graverini. Flavour anomalies: a review. *J. Phys. Conf. Ser.*, 1137(1):012025, 2019, 1807.11373.
- [35] Admir Greljo and David Marzocca. High- p_T dilepton tails and flavor physics. *Eur. Phys. J.*, C77(8):548, 2017, 1704.09015.
- [36] Andrzej J. Buras, Fulvia De Fazio, and Jennifer Girschbach. 331 models facing new $b \rightarrow s\mu^+\mu^-$ data. *JHEP*, 02:112, 2014, 1311.6729.
- [37] Rodrigo Alonso, Benjamín Grinstein, and Jorge Martin Camalich. Lepton universality violation and lepton flavor conservation in B -meson decays. *JHEP*, 10:184, 2015, 1505.05164.
- [38] Diego Guadagnoli, Dmitri Melikhov, and Meril Reboud. More Lepton Flavor Violating Observables for LHCb's Run 2. *Phys. Lett.*, B760:442–447, 2016, 1605.05718.
- [39] R. Sekhar Chivukula, Joshua Isaacson, Kirtimaan A. Mohan, Dipan Sengupta, and Elizabeth H. Simmons. R_K anomalies and simplified limits on Z' models at the LHC. *Phys. Rev.*, D96(7):075012, 2017, 1706.06575.
- [40] T. Hurth, F. Mahmoudi, D. Martinez Santos, and S. Neshatpour. Lepton nonuniversality in exclusive $b \rightarrow s\ell\ell$ decays. *Phys. Rev.*, D96(9):095034, 2017, 1705.06274.
- [41] Jorge Alda, Jaume Guasch, and Siannah Penaranda. Some results on Lepton Flavour Universality Violation. *Eur. Phys. J.*, C79(7):588, 2019, 1805.03636.
- [42] Steven Weinberg. Baryon and Lepton Nonconserving Processes. *Phys. Rev. Lett.*, 43:1566–1570, 1979.
- [43] Wolfgang Altmannshofer, P. S. Bhupal Dev, and Amarjit Soni. $R_{D^{(*)}}$ anomaly: A possible hint for natural supersymmetry with R -parity violation. *Phys. Rev.*, D96(9):095010, 2017, 1704.06659.
- [44] Yoav Afik, Jonathan Cohen, Eitan Gozani, Enrique Kajomovitz, and Yoram Rozen. Establishing a Search for $b \rightarrow s\ell^+\ell^-$ Anomalies at the LHC. *JHEP*, 08:056, 2018, 1805.11402.
- [45] Wolfgang Altmannshofer, P.S. Bhupal Dev, Amarjit Soni, and Yicong Sui. Addressing $R_{D^{(*)}}$, $R_{K^{(*)}}$, muon $g - 2$ and ANITA anomalies in a minimal R -parity violating supersymmetric framework. 2 2020, 2002.12910.
- [46] Darius A. Faroughy, Admir Greljo, and Jernej F. Kamenik. Confronting lepton flavor universality violation in B decays with high- p_T tau lepton searches at LHC. *Phys. Lett.*, B764:126–134, 2017, 1609.07138.
- [47] Javier Fuentes-Martin, Admir Greljo, Jorge Martin Camalich, and Jose David Ruiz-Alvarez. Charm Physics Confronts High- p_T Lepton Tails. 3 2020, 2003.12421.
- [48] Johan Alwall, Michel Herquet, Fabio Maltoni, Olivier Mattelaer, and Tim Stelzer. MadGraph 5 : Going Beyond. *JHEP*, 06:128, 2011, 1106.0522.
- [49] Adam Alloul, Neil D. Christensen, Céline Degrande, Claude Duhr, and Benjamin Fuks. FeynRules 2.0 - A complete toolbox for tree-level phenomenology. *Comput. Phys. Commun.*, 185:2250–2300, 2014, 1310.1921.
- [50] A. D. Martin, W. J. Stirling, R. S. Thorne, and G. Watt. Parton distributions for the LHC. *Eur. Phys. J.*, C63:189–285, 2009, 0901.0002.
- [51] Eric Conte, Benjamin Fuks, and Guillaume Serret. MadAnalysis 5, A User-Friendly Framework for Collider Phenomenology. *Comput. Phys. Commun.*, 184:222–256, 2013, 1206.1599.
- [52] Yoav Afik, Shaouly Bar-Shalom, Jonathan Cohen, and Yoram Rozen. Searching for New Physics with $b\bar{b}\ell^+\ell^-$ Contact Interactions. *Phys. Lett. B*, 807:135541, 2020, 1912.00425.
- [53] Albert M Sirunyan et al. Search for leptoquarks coupled to third-generation quarks in proton-proton collisions at $\sqrt{s} = 13$ TeV. *Phys. Rev. Lett.*, 121(24):241802, 2018, 1809.05558.
- [54] Shaouly Bar-Shalom, Jonathan Cohen, Amarjit Soni, and Jose Wudka. Phenomenology of TeV-scale scalar Leptoquarks in the EFT. *Phys. Rev.*, D100(5):055020, 2019, 1812.03178.
- [55] Morad Aaboud et al. Search for new high-mass phenomena in the dilepton final state using 36 inverse fb of proton-proton collision data at $\sqrt{s} = 13$ TeV with the ATLAS detector. *JHEP*, 10:182, 2017, 1707.02424.
- [56] Albert M Sirunyan et al. Search for third-generation scalar leptoquarks and heavy right-handed neutrinos in final states with two tau leptons and two jets in proton-proton collisions at $\sqrt{s} = 13$ TeV. *JHEP*, 07:121, 2017, 1703.03995.
- [57] Search for physics beyond the standard model in events with two same-sign leptons or at least three leptons and jets in proton-proton collisions at $\sqrt{s} = 13$ TeV. 3 2019.
- [58] Peter Tornambe. SUSY searches at $\sqrt{s} = 13$ TeV with two same-sign leptons or three leptons, jets and E_T^{miss} at the ATLAS detector - Background estimation and latest analysis results. *PoS, EPS-HEP2017:721*, 2018.
- [59] The ATLAS collaboration. Search for new phenomena with top quark pairs in final states with one lepton, jets, and missing transverse momentum in pp collisions at $\sqrt{s} = 13$ TeV with the ATLAS detector. 2 2020.
- [60] Morad Aaboud et al. Search for top-squark pair production in final states with one lepton, jets, and missing transverse momentum using 36 fb $^{-1}$ of $\sqrt{s} = 13$ TeV pp collision data with the ATLAS detector. *JHEP*, 06:108, 2018, 1711.11520.
- [61] Morad Aaboud et al. Searches for scalar leptoquarks and differential cross-section measurements in dilepton-dijet events in proton-proton collisions at a centre-of-mass energy of $\sqrt{s} = 13$ TeV with the ATLAS experiment. *Eur. Phys. J. C*, 79(9):733, 2019, 1902.00377.
- [62] Morad Aaboud et al. Search for a scalar partner of the top quark in the jets plus missing transverse momentum final state at $\sqrt{s}=13$ TeV with the ATLAS detector. *JHEP*, 12:085, 2017, 1709.04183.

- [63] Morad Aaboud et al. Search for dark matter produced in association with bottom or top quarks in $\sqrt{s} = 13$ TeV pp collisions with the ATLAS detector. *Eur. Phys. J. C*, 78(1):18, 2018, 1710.11412.
- [64] Albert M Sirunyan et al. Search for dark matter produced in association with a single top quark or a top quark pair in proton-proton collisions at $\sqrt{s} = 13$ TeV. *JHEP*, 03:141, 2019, 1901.01553.
- [65] K. Ackerstaff et al. Tests of the standard model and constraints on new physics from measurements of fermion pair production at 130-GeV to 172-GeV at LEP. *Eur. Phys. J.*, C2:441–472, 1998, hep-ex/9708024.
- [66] G. Abbiendi et al. Tests of the standard model and constraints on new physics from measurements of fermion pair production at 183-GeV at LEP. *Eur. Phys. J.*, C6:1–18, 1999, hep-ex/9808023.
- [67] R. Barate et al. Study of fermion pair production in e^+e^- collisions at 130-GeV to 183-GeV. *Eur. Phys. J.*, C12:183–207, 2000, hep-ex/9904011.
- [68] S. Schael et al. Fermion pair production in e^+e^- collisions at 189-209-GeV and constraints on physics beyond the standard model. *Eur. Phys. J.*, C49:411–437, 2007, hep-ex/0609051.
- [69] Radja Boughezal, Chien-Yi Chen, Frank Petriello, and Daniel Wiegand. Top quark decay at next-to-leading order in the Standard Model Effective Field Theory. *Phys. Rev. D*, 100(5):056023, 2019, 1907.00997.
- [70] Mikael Chala, Jose Santiago, and Michael Spannowsky. Constraining four-fermion operators using rare top decays. *JHEP*, 04:014, 2019, 1809.09624.

Appendix A: Distributions: bounds and discovery

In Fig. 3 we plot the distributions of the best fitted values of $1/\Lambda$ for the operator $\mathcal{O}_{\mu q_3}^{(3)}(2233)$, that minimize the χ^2 -test by mimicking a realistic setting with $\mathcal{O}(10000)$ random realizations of the experimental values for the LFNU ratios $T_{\ell\ell}^{mnp} = 1$, i.e., corresponding to the SM value, and normally distributed with the three uncertainty scenarios: $\delta T = 10\%$, 15% , 20% which correspond to the three systematic uncertainty choices outlined in the paper. The distributions are shown for $\mathcal{L} = 140 \text{ fb}^{-1}$ and the selection $m_{\ell\ell}^{\text{min}} = 300 \text{ GeV}$, $\mathcal{L} = 300 \text{ fb}^{-1}$ and the selection $m_{\ell\ell}^{\text{min}} = 400 \text{ GeV}$ and $\mathcal{L} = 3000 \text{ fb}^{-1}$ with the selection $m_{\ell\ell}^{\text{min}} = 700 \text{ GeV}$. The 95%CL bounds on Λ are then extracted from these distributions.

In Figs. 4 we plot the distributions of the best fitted values of Λ for both the operators $\mathcal{O}_{lq}^{(3)}(2233)$ and $\mathcal{O}_{qe}(2233)$, that minimize the χ^2 -test with $\mathcal{O}(10000)$ random realizations of the experimental measured ratios $T_{\ell\ell}^{\text{exp}}$, corresponding to the case where the NP is assumed in the data with specific values of $\bar{\Lambda}$, i.e., $T_{\ell\ell}^{\text{exp}} = T_{\ell\ell}(\bar{\Lambda})$, and normally distributed with two uncertainty scenarios: $\delta T = 10\%$ (case 1) and $\delta T = 20\%$ (case 3). That is, the experimental values $T_{\ell\ell}^{\text{exp}}$ are simulated $\mathcal{O}(10000)$ times from the normal distribution:

$$T_{\ell\ell}^{X,\text{exp}} = \mathcal{N}\left(T_{\ell\ell}^X(\bar{\Lambda}), (\delta T^X)^2\right), \quad (\text{A1})$$

where $X \in (mnp)$ denotes the di-lepton + jets production channels, and for each realization we find the best fitted value of Λ .

The distributions are shown In Figs. 4 for values of $\bar{\Lambda}$ that can be discovered at 5σ at the HL-LHC with $\mathcal{L} = 3000 \text{ fb}^{-1}$ and with the selection of $m_{\ell\ell}^{\text{min}} = 700 \text{ GeV}$.

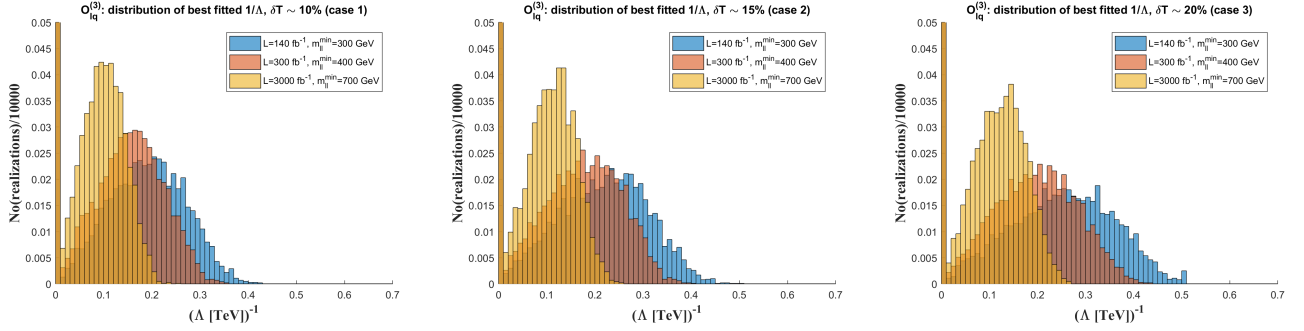


FIG. 3: The normalized distribution of the inverse value of the best fitted Λ of the operator $\mathcal{O}_{\mu q_3}^{(3)} = (\bar{\mu}\gamma_\mu\tau^I\mu)(\bar{q}_3\gamma^\mu\tau^I q_3)$, that minimize the χ^2 -test with $T_{\ell\ell}^{\text{exp}} = 1$, i.e., corresponding to the SM value, and normally distributed with the three uncertainty scenarios: $\delta T = 10\%$ (left), $\delta T = 15\%$ (middle) and $\delta T = 20\%$ (right). See also text.

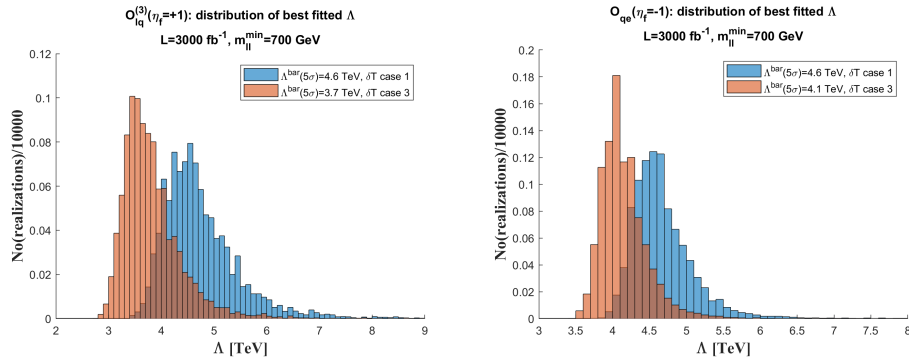


FIG. 4: The normalized distribution of the best fitted Λ of the operators $\mathcal{O}_{lq_3}^{(3)}(2233)$ (left) and $\mathcal{O}_{qe}(2233)$ (right), that minimize the χ^2 -test with $T_{\ell\ell}^{\text{exp}} = T_{\ell\ell}(\bar{\Lambda})$, i.e., corresponding to the case where the NP is assumed in the data with specific values of $\bar{\Lambda}$ (as indicated) and normally distributed with two uncertainty scenarios: $\delta T = 10\%$ (case 1) and $\delta T = 20\%$ (case 3). See also text.

Supplemental material

I. POTENTIAL LFNU DIMENSION SIX OPERATORS IN THE SMEFT

In Table I we list all the dimension six operators in the SMEFT framework that can potentially violate LFU and that are, therefore, relevant to our study; operators with four leptons are excluded. We also assume that baryon number is conserved in the underlying heavy theory.

TABLE I: The potentially lepton non-universal dimension six operators in the SMEFT (see also text). The subscripts p, r, s, t are flavor indices.

Higgs-Lepton scalar	Higgs-Lepton vector	Lepton MDM
$\mathcal{O}_{eH}(pr) \left (H^\dagger H)(\bar{l}_p e_r H) \right.$	$\mathcal{O}_{Hl}^{(1)}(pr) \left (H^\dagger i \overleftrightarrow{D}_\mu H)(\bar{l}_p \gamma^\mu l_r) \right.$	$\mathcal{O}_{eW}(pr) \left (\bar{l}_p \sigma^{\mu\nu} e_r) \tau^I H W_{\mu\nu}^I \right.$
	$\mathcal{O}_{Hl}^{(3)}(pr) \left (H^\dagger i \overleftrightarrow{D}_\mu^I H)(\bar{l}_p \tau^I \gamma^\mu l_r) \right.$	$\mathcal{O}_{eB}(pr) \left (\bar{l}_p \sigma^{\mu\nu} e_r) H B_{\mu\nu} \right.$
	$\mathcal{O}_{He}(pr) \left (H^\dagger i \overleftrightarrow{D}_\mu H)(\bar{e}_p \gamma^\mu e_r) \right.$	
4 – Fermi : $(\bar{L}L)(\bar{L}L)$	4 – Fermi : $(\bar{R}R)(\bar{R}R)$	4 – Fermi : $(\bar{L}L)(\bar{R}R)$
$\mathcal{O}_{lq}^{(1)}(prst) \left (\bar{l}_p \gamma_\mu l_r)(\bar{q}_s \gamma^\mu q_t) \right.$	$\mathcal{O}_{eu}(prst) \left (\bar{e}_p \gamma_\mu e_r)(\bar{u}_s \gamma^\mu u_t) \right.$	$\mathcal{O}_{lu}(prst) \left (\bar{l}_p \gamma_\mu l_r)(\bar{u}_s \gamma^\mu u_t) \right.$
$\mathcal{O}_{lq}^{(3)}(prst) \left (\bar{l}_p \gamma_\mu \tau^I l_r)(\bar{q}_s \gamma^\mu \tau^I q_t) \right.$	$\mathcal{O}_{ed}(prst) \left (\bar{e}_p \gamma_\mu e_r)(\bar{d}_s \gamma^\mu d_t) \right.$	$\mathcal{O}_{ld}(prst) \left (\bar{l}_p \gamma_\mu l_r)(\bar{d}_s \gamma^\mu d_t) \right.$
		$\mathcal{O}_{qe}(prst) \left (\bar{q}_p \gamma_\mu q_r)(\bar{e}_s \gamma^\mu e_t) \right.$
4 – Fermi : $(\bar{L}R)(\bar{R}L) + \text{h.c.}$	4 – Fermi : $(\bar{L}R)(\bar{L}R) + \text{h.c.}$	
$\mathcal{O}_{ledq}(prst) \left (\bar{l}_p^j e_r)(\bar{d}_s q_{tj}) \right.$	$\mathcal{O}_{lequ}^{(1)}(prst) \left (\bar{l}_p^j e_r) \epsilon_{jk} (\bar{q}_s^k u_t) \right.$	
	$\mathcal{O}_{lequ}^{(3)}(prst) \left (\bar{l}_p^j \sigma_{\mu\nu} e_r) \epsilon_{jk} (\bar{q}_s^k \sigma^{\mu\nu} u_t) \right.$	

II. DISTRIBUTIONS: BOUNDS AND DISCOVERY

In Fig. 1 we plot the distributions of the best fitted values of $1/\Lambda$ for the operator $\mathcal{O}_{\mu q_3}^{(3)}(2233)$, that minimize the χ^2 -test by mimicking a realistic setting with $\mathcal{O}(10000)$ random realizations of the experimental values for the LFNU ratios $T_{\ell\ell}^{mnp} = 1$, i.e., corresponding to the SM value, and normally distributed with the three uncertainty scenarios: $\delta T = 10\%, 15\%, 20\%$ which correspond to the three systematic uncertainty choices outlined in the paper. The distributions are shown for $\mathcal{L} = 140 \text{ fb}^{-1}$ and the selection $m_{\ell\ell}^{min} = 300 \text{ GeV}$, $\mathcal{L} = 300 \text{ fb}^{-1}$ and the selection $m_{\ell\ell}^{min} = 400 \text{ GeV}$ and $\mathcal{L} = 3000 \text{ fb}^{-1}$ with the selection $m_{\ell\ell}^{min} = 700 \text{ GeV}$. The 95%CL bounds on Λ are then extracted from these distributions.

In Figs. 2 we plot the distributions of the best fitted values of Λ for both the operators $\mathcal{O}_{\ell q}^{(3)}(2233)$ and $\mathcal{O}_{qe}(2233)$, that minimize the χ^2 -test with $\mathcal{O}(10000)$ random realizations of the experimental measured ratios $T_{\ell\ell}^{exp}$, corresponding to the case where the NP is assumed in the data with specific values of $\bar{\Lambda}$, i.e., $T_{\ell\ell}^{exp} = T_{\ell\ell}(\bar{\Lambda})$, and normally distributed with two uncertainty scenarios: $\delta T = 10\%$ (case 1) and $\delta T = 20\%$ (case 3). That is, the experimental values $T_{\ell\ell}^{exp}$ are simulated $\mathcal{O}(10000)$ times from the normal distribution:

$$T_{\ell\ell}^{X,exp} = \mathcal{N} \left(T_{\ell\ell}^X(\bar{\Lambda}), (\delta T^X)^2 \right), \quad (1)$$

where $X \in (mnp)$ denotes the dilepton + jets production channels, and for each realization we find the best fitted value of Λ .

The distributions are shown In Figs. 2 for values of $\bar{\Lambda}$ that can be discovered at 5σ at the HL-LHC with $\mathcal{L} = 3000 \text{ fb}^{-1}$ and with the selection of $m_{\ell\ell}^{min} = 700 \text{ GeV}$.

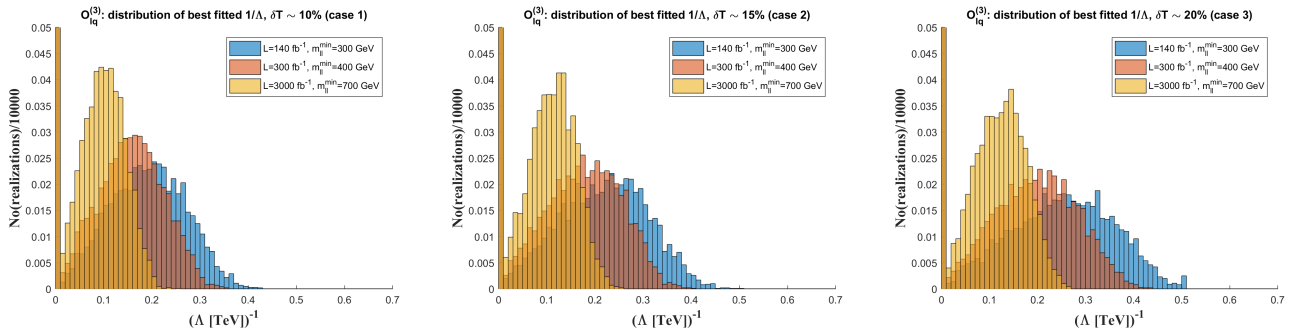


FIG. 1: The normalized distribution of the inverse value of the best fitted Λ of the operator $\mathcal{O}_{\mu q_3}^{(3)} = (\bar{\mu}\gamma_\mu\tau^I\mu)(\bar{q}_3\gamma^\mu\tau^I q_3)$, that minimize the χ^2 -test with $T_{\ell\ell}^{exp} = 1$, i.e., corresponding to the SM value, and normally distributed with the three uncertainty scenarios: $\delta T = 10\%$ (left), $\delta T = 15\%$ (middle) and $\delta T = 20\%$ (right). See also text.

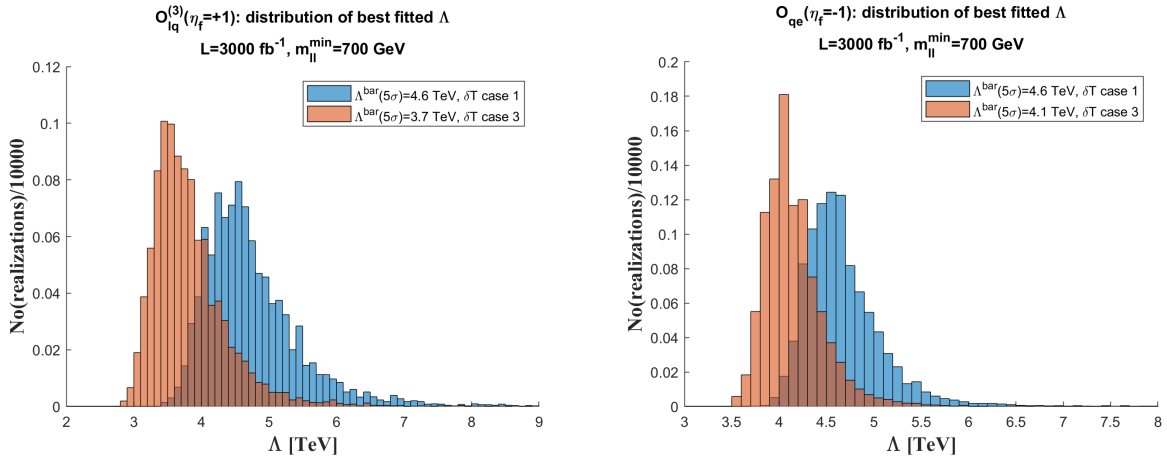


FIG. 2: The normalized distribution of the best fitted Λ of the operators $\mathcal{O}_{lq_3}^{(3)}$ (2233) (left) and \mathcal{O}_{qe} (2233) (right), that minimize the χ^2 -test with $T_{\ell\ell}^{exp} = T_{\ell\ell}(\bar{\Lambda})$, i.e., corresponding to the case where the NP is assumed in the data with specific values of $\bar{\Lambda}$ (as indicated) and normally distributed with two uncertainty scenarios: $\delta T = 10\%$ (case 1) and $\delta T = 20\%$ (case 3). See also text.